NANO LETTERS

LETTER

pubs.acs.org/NanoLett

Discrete Dynamics of Nanoparticle Channelling in Suspended Graphene

Tim J. Booth,*[,†] Filippo Pizzocchero,[†] Henrik Andersen,[†] Thomas W. Hansen,[‡] Jakob B. Wagner,[‡] Joerg R. Jinschek,[§] Rafal E. Dunin-Borkowski,[‡] Ole Hansen,[†] and Peter Bøggild[†]

[†]DTU Nanotech, Kgs. Lyngby, Denmark

[‡]DTU CEN, Kgs. Lyngby, Denmark

[§]FEI Company bb. Eindhoven, The Netherlands

Supporting Information

ABSTRACT: We have observed a previously undescribed stepwise oxidation of mono- and few layer suspended graphene by silver nanoparticles in situ at subnanometer scale in an environmental transmission electron microscope. Over the range of 600−850 K, we observe crystallographically oriented channelling with rates in the range 0.01−1 nm/s and calculate an activation energy of 0.557 ± 0.016 eV. We present a discrete statistical model for this process and discuss the implications for accurate nanoscale patterning of nanoscale systems.

KEYWORDS: Graphene, graphene membranes, silver nanoparticles, catalysis, channelling

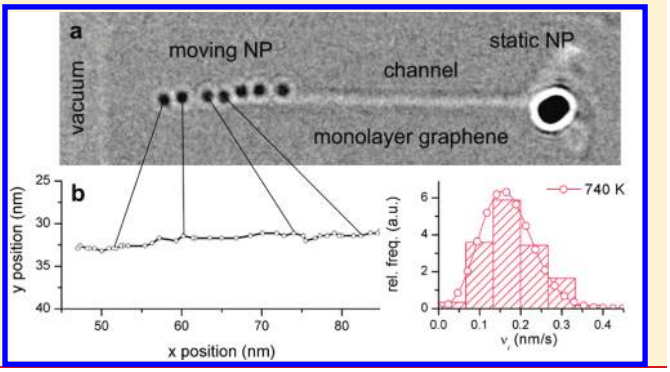

The channelling of graphite by metal nanoparticles in oxidizing or reducing environments has been the subject of intermittent interest since the discovery of the effect in the 1930s.[1−9] Recently, the potential of this method for the patterning of graphene has been discussed[10−16] due to a number of inherent advantages over the application of standard silicon microfabrication techniques to graphene: channelling is directed along well-defined crystal lattice directions (usually the so-called "zig-zag" or "armchair") with channel widths determined by the particle diameter, low edge roughness (<1 nm), the avoidance of resist masks combined with the possibility of parallel fabrication. While these features are all unique to nanoparticle channelling in graphene[16] the preference for certain crystallographic orientations is perhaps the most interesting. This is so far the only known method of patterning graphene along particular crystallographic directions to leave edges consisting of a single chirality which is crucial for graphene nanoribbon and spintronics devices.[17]

All previous studies of channelling behavior have been limited by the need to perform the experiment ex situ, that is, comparing single "before" and "after" images; for example, observation of the oxidation of graphene layers supported by the graphite basal plane by silver nanoparticles ex situ at 900 K in air,[12] or hydrogenation of monolayer graphene supported by oxidized silicon ex situ at 1300 K under a flow of hydrogen.[13] In these and other ex situ experiments, the dynamic behavior must be inferred from the length of channels and heating time after completion of the experiment with the rate of formation of the channel assumed to be consistent over the course of the experiment.

Here, we report for the first time the nanoscale observation of this channelling process by silver nanoparticles in an oxygen atmosphere in situ on suspended mono- and bilayer graphene in an environmental transmission electron microscope, enabling direct concurrent observation of the process, which is impossible in ex situ experiments. The use of suspended graphene membranes of large area and known number of layers is an advantage for the analysis of behavior. In contradiction to the constant velocity assumed in all previous reports, the velocity varies randomly on short length and time scales, even including some lateral motion. We are able to determine reliably the ensemble activation energy for the process based on the velocity distributions. Measurement of the particle velocities in situ in the ETEM is the first demonstrated accurate way to determine the activation energy for this process.

Over the temperature range 600−850K at oxygen flow rates of 2−10 mL/min, we have measured particle channelling rates of 0.01−1 nm/s for more than 25 particles. Via analysis of diffraction patterns and high-resolution images, we find that all of the channels in monolayer and bilayer graphene longer than the particle diameter are aligned to the ⟨100⟩ directions in graphene, that is, leaving zigzag edges behind (Figure 1e,f). The edge roughness of etched channels appears to be smaller than 1 nm with more accurate determination of the roughness limited by the constant removal of undercoordinated edge atoms via knock-on damage during imaging.[18]

The particles move at a surprisingly uneven rate, even when making long straight channels (Figure 2a). In addition, the particles exhibit a small degree of fluctuating motion normal to the channelling direction. At 600 K the etching rate is slow with

Received: March 21, 2011
Revised: May 16, 2011
Published: June 09, 2011

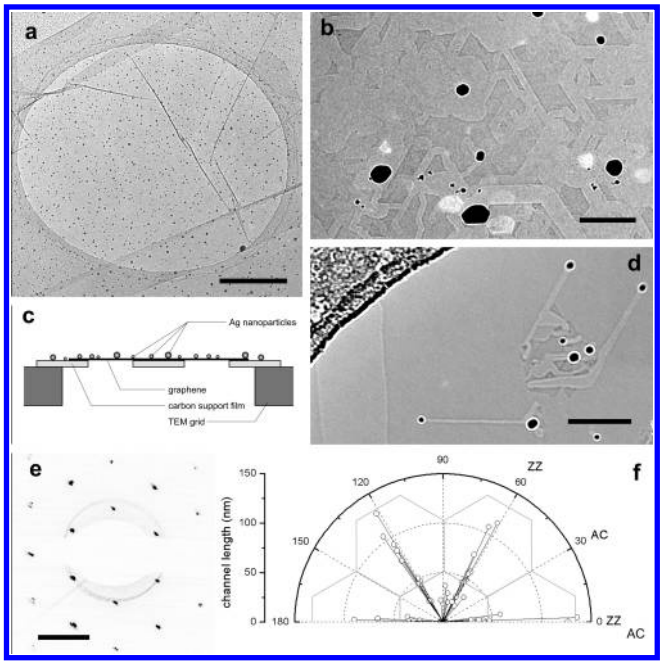

Figure 1. (a) Transmission electron microscopy (TEM) micrograph of an aperture with suspended few layer graphene after evaporation of Ag (visible as dark spots). Holey carbon support film is visible at the edges of the image. Scale bar 500 nm. (b) Few layer suspended graphene film showing numerous channels. Defocus is used to emphasize the channel edges and highlight the Bragg reflections of the crystalline silver nanoparticles (bright spots). Scale bar 100 nm. (c) Diagram of sample construction. (d) Multiple nanoparticles channelling through a monolayer graphene sheet. Carbon support film and the edges of the graphene sheet are visible at the left of the image. Scale bar 100 nm. (e) Single layer graphene diffraction pattern of panel d. Scale bar 5 nm^{-1}. (f) Polar plot of channel length and orientation for a typical image. The orientation of the graphene lattice is indicated.

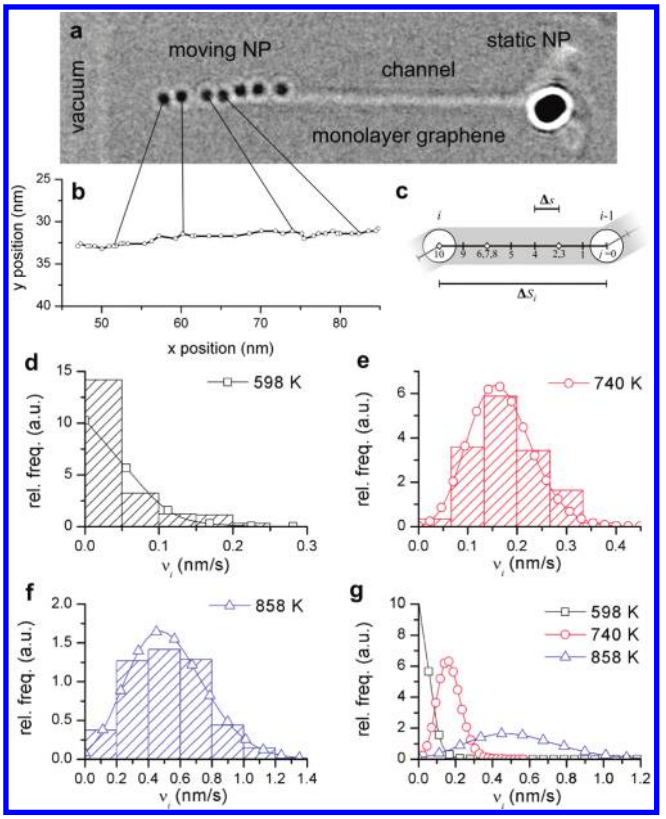

Figure 2. (a) Individual nanoparticle channelling in monolayer graphene. Seven frames are superimposed with a time between successive frames of 124 s. The particle eventually reaches the graphene edge indicated and the graphene sheet is cut (see Supporting Information). (b) The positions of the particle in panel a, measured every 12.4 s. The variation in the particle displacement between successive intervals of time is clear. (c) Schematic of the model. The total displacement ΔS_i of the particle in the ith interval is measured after a period of time $\Delta\tau \gg \Delta t$. In the diagram, $\Delta\tau/\Delta t = N = 10$. At each moment Δt_j the particle can either move a discrete distance Δs with probability x or remain stationary with probability $1 - x$. Each interval $\Delta\tau$ contains an average of xN movements of Δs. (d–f) Selected histograms of the interval velocities for three different particles at different temperatures, T = 598, 740, and 858 K. The points overlaid are the x-scaled Poisson distribution corresponding to integer values of $k = \{1, 2, ...\}$. The histograms and models are normalized to 1. The lines are guides for the eye. (g) Comparison of the models from (d–f); note the increase in variance with temperature.

the particles appearing stationary in many intervals (to within a single pixel) (Figure 2d). The mean and variance of the channelling rates increase at higher temperatures with notably fewer stationary periods (Figure 2e–g).

To explain this erratic behavior, we propose a discrete model of the particle motion by introducing a scale time Δt and scale distance Δs. The position of the particle either changes instantaneously by Δs with probability $P(\text{move}) = x$, or is otherwise stationary. The position of the particle is measured at equal time intervals of length $\Delta\tau$ providing $N = \Delta\tau/\Delta t \gg 1$ successive independent tests during that interval, with $n_i \leq N$ discrete steps accounting for the total movement of the particle ΔS_i during the ith interval of length $\Delta\tau$. The expectation value for the number of movements during the interval is xN. We define the interval velocity $v_i = \Delta S_i/\Delta\tau = n_i\Delta S/\Delta\tau$.

The probability of observing exactly k movements for N successive tests is then given by the Poisson distribution

$$\text{Poisson}(n_i = k; xN) = (xN)^k \frac{\exp(-xN)}{k!}$$

Sampling the interval velocity of the particle over M intervals gives a set of velocities $\{\Delta v_1, \Delta v_2, ...\Delta v_M\}$. The average $\bar{v}$ of this set

$$\bar{v} = \frac{\sum_{i=1}^{M} v_i}{M}$$

is the maximum likelihood estimator of the most likely velocity $\tilde{v}$ of the particle. For large enough M

$$\bar{v} \cong \tilde{v} = xN\frac{\Delta s}{\Delta\tau} = x\frac{\Delta s}{\Delta t} = Kx$$

giving a scale velocity K for the system.

If we assume that the probability of a single discrete motion depends on temperature as $x = \exp(-E_a/k_BT)$ and plot experimental velocity estimates $\bar{v}$ in an Arrhenius plot $\ln(\bar{v}/v_0) = \ln(K/v_0) - E_a/k_BT$ (where v_0 = 1 nm/s) as a function of T^{-1} then linear regression provides an estimate of the y-intercept $\ln(K/v_0)$ and the gradient $-E_a/k_B$. We obtain $K = 1.8 \pm 0.5\ \mu m\ s^{-1}$ and $E_a = 0.557 \pm 0.016$ eV (Figure 3a). Scaling the Poisson distribution by our experimentally determined K and our measurement interval $\Delta\tau$ and setting Δs = 1.4 Å, the interatomic distance in graphene, we obtain excellent agreement between the predicted

dx.doi.org/10.1021/nl200928k |Nano Lett. 2011, 11, 2689–2692

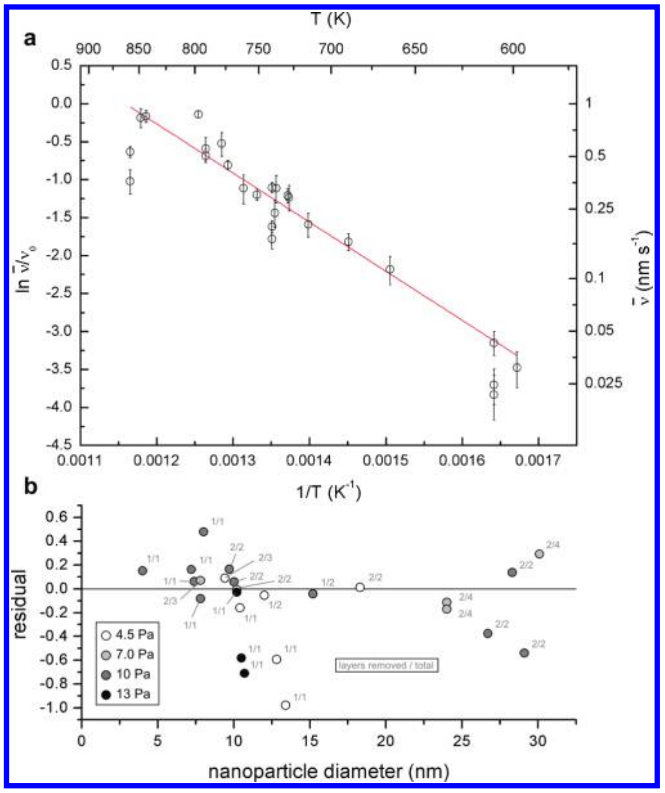

Figure 3. (a) Arrhenius plot of $\ln(\bar{v}/v_0)$ vs T^{-1}. Linear regression gives E_a and the prefactor K by $\ln(\bar{v}/v_0) = \ln(K/v_0) - E_a/k_BT$. Error bars account for both statistical uncertainty and pixel quantization. (b) Plot of residuals from fit in panel a vs nanoparticle diameter. By eliminating the effect of temperature on velocity, we observe no correlation of velocity with diameter. The gray level of the point indicates the pressure, and the labels show the number of removed layers and the total number, that is, 1/1 indicates monolayer channelling, 1/2 indicates one layer of a bilayer, etc. No correlation is observed for either variable. The horizontal line indicates the calculated regression line in panel a.

and experimentally sampled frequencies of the interval velocities (Figure 2d−g). $K/\Delta s$ gives an estimate of Δt of 80 ± 20 μs. We stress that we have not fit the data to a Poisson distribution and do not use any free parameters except for assuming that Δs = 1.4 Å is the scale length of the smallest discrete motion. The randomized, discontinuous motion described in this model and observed experimentally is analogous to shot noise in electronics. We also note that due to the properties of the Poisson distribution, the standard deviation of the velocity $\sigma_{\tilde{v}} \sim (x)^{1/2} \sim \exp(-E_a/2k_BT)$, and therefore increases quite rapidly at first with increasing temperature.

We observe some completely stationary particles, which supports the idea that channelling in the investigated system only initiates at defect sites on the graphene surface or edges.[12] The alignment of the channels to the ⟨100⟩ directions in graphene indicates that the removal of "armchair" carbon atoms is energetically favorable, as compared to "zigzag" atoms, which end up comprising the edges of the channels. The mean particle velocities display a marked lack of dependence on the number of layers that are removed or particle size (Figure 3b) and in contrast to previous reports.[7] We ascribe this behavior to a nearly constant number density of carbon atoms per silver atom per unit of contact perimeter of the particle with the graphene. There is also no apparent dependence on the flow rate, and hence the pressure of oxygen, within the range tested (Figure 3b). In contrast to previous reports,[12] we do not observe any spiralling behavior, which can possibly be ascribed to the lack of a substrate, for example, misoriented graphite basal planes in a bulk HOPG crystal. Alternatively, spiralling behavior may be limited to particles larger than observed here.

We have performed in situ observation of the catalytic channelling behavior of silver nanoparticles on a suspended graphene surface for the first time. By performing the experiment in situ, the particle position can be monitored during the formation of the channel, in contrast to ex situ experiments. We find particle velocities of 0.01−1 nm/s over the temperature range 600−850 K at pressures of 4.5−13 Pa, which is in contrast to the rapid 250 nm/s at 900 K in air as previously reported.[12]

Sampling the position of the particle with greater temporal and spatial resolution enables us to observe small lateral deviations of the particle around the main direction of motion; accounting for these lateral deviations enables more accurate determination of the average particle velocity. The channelling direction of the particles is aligned to the ⟨100⟩ directions, driven by the difference in energy required to remove individual atoms from the receding edge. The particles move with a discrete stop−start motion, leading to an overall velocity whose distribution is well described by the Poisson distribution. As a direct consequence, $\sigma^2_{\tilde{v}}$ scales in direct proportion to $\tilde{v}$. This may pose problems when using many particles in parallel to channel graphene, since the particles will not move at identical velocities. The proportional standard deviation $\sigma_{\tilde{v}}/\tilde{v} \propto x^{-1/2}$ indicates that higher temperatures could remedy this problem by reducing the relative effect. This uncertainty is a fundamental feature of discrete systems and leads to unavoidable variations when dealing with the small numbers of atoms which are important at the nanoscale.

We have determined the ensemble activation energy for the process at 0.557 ± 0.016 eV. This is the first time that the activation energy has been calculated for this process by in situ observation of the actual particle dynamics.

Catalytic particle channelling has unique possibilities in terms of providing lithographic patterning on a scale much smaller than any other nonserial technique and has the outstanding quality that the crystallographic directions are automatically selected with no need of subsequent annealing or postprocessing[19] or for prior knowledge of the lattice orientation. The channels could be utilized as self-aligned, batch-fabricated electrode gaps with dimensions in a relevant range for molecular electronics, where electrode faces with Å-level ordering appear to be within reach.

Methods. *Sample Preparation.* Graphene was prepared on 90 nm poly(methyl methacrylate) (PMMA)-coated silicon substrates and either transferred to Quantifoil TEM grids,[20] or a TEM grid produced in place by electroplating.[21] These procedures result in multiple freestanding graphene regions with a size in excess of 2 μm supported at the periphery (Figure 1a,c).

The samples were inserted into a TEM sample holder with an Inconel heating element (Gatan Inc.) and were baked out at 770 K at 10^{-4} Pa for a minimum of 5 h to reduce hydrocarbon contamination from oil and resist residues. We note that the electron beam will cross-link residual PMMA, making it more difficult to remove via annealing if the sample is exposed to the electron beam before this cleaning process is complete.

After cleaning, an amount of silver equivalent to a 0.1−1 Å layer is sputtered onto the entire sample surface ex situ. At such low coverage, we readily observe nanoparticles with sizes of the order of 10 nm on the graphene surface. At higher silver coverage

dx.doi.org/10.1021/nl200928k |*Nano Lett.* 2011, 11, 2689–2692

(~5 Å), the particles first oxidize surfacial hydrocarbon contamination rather than graphene. Once the contamination is removed, however, the graphene sheet is very rapidly destroyed (Supporting Information Video S1a and Video S1b).

Imaging Conditions. The samples are imaged at 80 keV in a spherical aberration corrected FEI Titan ETEM. To initiate the channelling behavior, we introduce oxygen at a flow rate of 2−10 mL/min, resulting in a pressure of 4.5−13 Pa in the immediate vicinity of the sample. This leads to a strong thermally induced drift of the sample. For this reason, it was not possible to make very accurate observations of the onset of channelling behavior, although the channelling appeared to start and stop immediately with the presence or absence of a flow of oxygen, respectively.

Particles that display channelling behavior (Figure 1b,d) are observed in the TEM with typically 200−1000 images taken at a measured framerate of ~0.1−1 Hz per particle (Supporting Information Video S2 and Figure S2). Drift correction, where necessary, is performed using automated image registration based on the SIFT technique;[22] briefly, key features are extracted from an image based on contrast and then identified in the next image in the sequence with the relative image translation used to compensate for the drift. We use magnifications of 10−87 kX, corresponding to 180−650 pm/px. The beam current is kept constant at 20 nA, but the intensity of the beam is varied to ensure adequate signal-to-noise ratio at different magnifications. No systematic variation in the particle behavior as a function of beam intensity is observed. A closer study is required to verify this, since momentum transfer to the particles cannot be ruled out as a contributing factor.[23,24]

Position Measurement. The (x,y) position of the centroid of the particle is measured every frame (Figure 2a,b), and the 2D displacement $\Delta S_i = [(x_i - x_{i-1})^2 + (y_i - y_{i-1})^2]^{1/2}$ during the interval $\Delta\tau$ is calculated (Figure 2c), resulting in a histogram of "interval velocity" $v_i = \Delta S_i/\Delta\tau$ (Figure 2d−g). Where necessary, the resolution of the images is doubled using bicubic interpolation, to reduce the influence of pixel quantization error on finding the centroid.

■ ASSOCIATED CONTENT

Supporting Information. Four movies (S1a (si_002.avi), S1b (si_003.avi), S2 (si_004.avi), S3 (si_005.avi)) of nanoparticle etching observed in situ and raw (x,y,t) data in spreadsheet form. This material is available free of charge via the Internet at http://pubs.acs.org.

■ AUTHOR INFORMATION

Corresponding Author
*E-mail: tim.booth@nanotech.dtu.dk.

■ ACKNOWLEDGMENT

Support from the Danish FTP project "Nanoengineered graphene devices" is gratefully acknowledged. The authors also gratefully acknowledge helpful discussions with A. M. Paganoni of the Politecnico di Milano.

■ REFERENCES

(1) Greer, E. N.; Topley, B. Attack of oxygen molecules upon highly crystalline graphite. *Nature* **1932**, *129*, 904–905.
(2) Hennig, G. R. Catalytic oxidation of graphite. *J. Inorg. Nucl. Chem.* **1962**, *24*, 1129–1132, IN1−IN4, 1133−1137.
(3) Hughes, G.; Thomas, J.; Marsh, H.; Reed, R. Origin of etch pits on graphite surfaces. *Carbon* **1964**, *1*, 339–343.
(4) Harris, P; et al. Controlled atmosphere electron microscopy studies of graphite gasification—4. Catalysis of the graphite-O_2 reaction by silver. *Carbon* **1974**, *12*, 189–197.
(5) Tomita, A.; Tamai, Y. Optical microscopic study on the catalytic hydrogenation of graphite. *J. Phys. Chem.* **1974**, *78*, 2254–2258.
(6) Baker, R. Catalytic oxidation of graphite by platinum and palladium. *J. Catal.* **1976**, *41*, 22–29.
(7) Goethel, P. J. Mechanism of catalyzed graphite oxidation by monolayer channeling and monolayer edge recession. *J. Catal.* **1989**, *119*, 201–214.
(8) Watanabe, H. Local etching effect of fine gold particles deposited on graphite. *Jpn. J. Appl. Phys.* **1993**, *32*, 2809–2813.
(9) Konishi, S; et al. Catalytic creation of channels in the surface layers of highly oriented pyrolytic graphite by cobalt nanoparticles. *Carbon* **2006**, *44*, 2338–2340.
(10) Ci, L.; et al. Controlled nanocutting of graphene. *Nano Res.* **2008**, *1*, 116–122.
(11) Datta, S. S.; et al. Crystallographic Etching of Few-Layer Graphene. *Nano Lett.* **2008**, *8*, 1912–1915.
(12) Severin, N; et al. Rapid Trench Channeling of Graphenes with Catalytic Silver Nanoparticles. *Nano Lett.* **2009**, *9*, 457–461.
(13) Campos, L. C.; et al. Anisotropic Etching and Nanoribbon Formation in Single-Layer Graphene. *Nano Lett.* **2009**, *9*, 2600–2604.
(14) Gao, L.; et al. Crystallographic Tailoring of Graphene by Nonmetal SiO_x Nanoparticles. *J. Am. Chem. Soc.* **2009**, *131* 13934–13936.
(15) Schäffel, F.; et al. On the catalytic hydrogenation of graphite for graphene nanoribbon fabrication. *Phys. Status Solidi B* **2009**, *246* 2540–2544.
(16) Biró, L. P. Nanopatterning of graphene with crystallographic orientation control. *Carbon* **2010**, *48*, 2677–2689.
(17) Ritter, K. A.; Lyding, J. W. The influence of edge structure on the electronic properties of graphene quantum dots and nanoribbons. *Nat. Mater.* **2009**, *8*, 235–242.
(18) Girit, C. O.; et al. Graphene at the edge: stability and dynamics. *Science* **2009**, *323*, 1705–1708.
(19) Jia, X.; et al. Controlled formation of sharp zigzag and armchair edges in graphitic nanoribbons. *Science* **2009**, *323*, 1701–1705.
(20) Meyer, J. C.; et al. Hydrocarbon lithography on graphene membranes. *Appl. Phys. Lett.* **2008**, *92*, 123110.
(21) Booth, T. J.; et al. Macroscopic Graphene Membranes and Their Extraordinary Stiffness. *Nano Lett.* **2008**, *8*, 2442–2446.
(22) Lowe, D. G. Distinctive image features from scale-invariant keypoints. *Int. J. Comput. Vision* **2004**, *60*, 91–110.
(23) Marks, L.; Zhang, J. Is there an electron wind?. *Ultramicroscopy* **1992**, *41*, 419–422.
(24) García de Abajo, F. Momentum transfer to small particles by passing electron beams. *Phys. Rev. B* **2004**, *70*, 115422.